THE JOURNAL OF PHYSICAL CHEMISTRY C
A JOURNAL OF THE AMERICAN CHEMICAL SOCIETY

pubs.acs.org/JPCC

Article

Tailoring Graphene Functionalization with Organic Residues for Selective Sensing of Nitrogenated Compounds: Structure and Transport Properties via QM Simulations

Sabrine Baachaoui, Luca Sementa, Rabiaa Hajlaoui, Sarah Aldulaijan, Alessandro Fortunelli,* Adnene Dhouib,* and Noureddine Raouafi*

Cite This: *J. Phys. Chem. C* 2023, 127, 15474−15485

Read Online

ACCESS | Metrics & More | Article Recommendations | Supporting Information

ABSTRACT: Graphene bearing organic functional groups chemically tethered to its surface *via* covalent bonds can find several applications in the sensing of gas, heavy metal ions, and other target species of interest. Herein, we used DFT simulations to study the thermodynamics of graphene functionalization with substituted carbenes, and the use of the resulting adducts to detect gaseous nitrogenated compounds—focusing on ammonia (NH_3), methylamine (MMA), dimethylamine (DMA), and trimethylamine (TMA). We find that the modified materials can interact with the amines, selectively also in the presence of other gases such as CO_2, SO_2, H_2S, and CH_4. Changes in the electronic properties of the system upon adsorption such as charge density, Löwdin partial charges, and projected density of states (PDOS) were used to analyze the interaction. Expected recovery times suggest that these nanomaterials can be used to detect the nitrogenated compounds here investigated at relatively low temperatures (298 and 373 K). Furthermore, by modeling the conductance of the functionalized graphene bare and in the presence of ammonia, we show that quantum conductance and the integrated currents are sensitive to functionalization and, importantly, to the presence of ammonia under determined conditions, which in principle allows tuning the sensitivity of the resulting device. Our work thus clarifies the principles governing this phenomenon. Carbene-functionalized graphene is concluded to be a potentially good candidate to replace noble-metal-modified graphene for the detection of ammonia/amines in chemoresistance or field-effect transistor-based sensors.

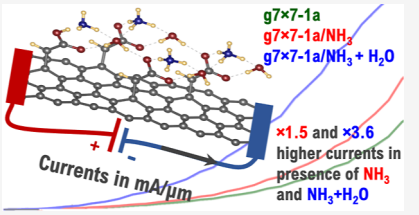

1. INTRODUCTION

In the current chemical production,[1] ammonia and other nitrogenated compounds are highly demanded to produce fertilizers, drugs, and pesticides to improve the quality of crops, to fight bacteria and invasive insects and herbs.[2] Ammonia and short-length chain amines are also often released by the decay of animals and spoiled fish, animal husbandry, and industrial plants.[3−5] Designing operative tools for their detection is thus an active field of research, especially if starting from cost-effective raw materials such as carbon nanomaterials.

Since fullerene was reported, for the first time in 1984, as a nanometric form of carbon,[6] considerable efforts have then been devoted to designing carbon-based gas sensors using fullerenes, carbon nanotubes, and graphene and graphene-like nanomaterials such as BC_3 and BC_6N, or MXenes.[7−10] In particular, graphene derivatives are commonly studied to design biosensors for the detection of various compound targets of interest and assess their level of applicability as (bio)markers for healthcare, food safety and environmental monitoring.[11−17] Numerous strategies have been devised for introducing functional groups (nitrile, carboxylic acid, thiol, amine, substituted acetylene derivatives, allyl and aryl groups, etc.) starting from insulating fluorographene using several classical organic reactions such as Sonogashira coupling, nucleophilic substitution and addition of organometallics.[18−22] Non-covalent approaches such as using 1-pyrenebutyric acid are routinely used to functionalize the graphene without disrupting its electronic cloud.[23−25] Several theoretical reports examined the functionalization of graphene with carbenes since it allows introducing organic functionalizer with specific properties.[26−31] This type of modification is reversible, indeed above 160 °C, functionalized graphene derivatives undergo retro Diels Alder reaction to retrieve the original graphene nanomaterials.[32−34] However, as far as we know, there is no previous report on the use of carbene-functionalized graphene derivatives for gas sensing. For instance, Zan examined the theoretical aspects of graphene functionalization with a series of symmetrical carbenes and showed that the chemical modification induced a bandgap opening of 0.25 to 0.58 eV.[31] Sainsbury et al. used dibromocarbene to modify graphene and the functionalized nanomaterial that was characterized by a palette of spectroscopic techniques to

Received: March 23, 2023
Revised: July 14, 2023
Published: July 29, 2023

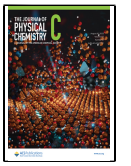

investigate the functionalization influence on the optical and electronic properties of the graphene, although not tested in sensing.[28] The graphene rippling effect on adsorption of various substances such as H_2, NH_2, and CO was also studied by many authors.[27,35−38] For instance, Hildebrand et al. elaborated a model to predict the changes of the physical properties of graphene after carbene adsorption.[27] They also showed that it is possible to modulate the bandgap using strain engineering by tethering carbenes on a graphene surface. Typically, adsorption releases an energy of up to 3.7 eV and induces distortion of the graphene with a rippling of energy around 1.4 eV.

Chemical modification of graphene surface by depositing metal nanoparticles[39−42] or adsorbing organic molecules[43−48] is an interesting path to build gas sensors. For instance, Baachaoui and co-workers demonstrated that the graphene derivatization with arylnitrenes induces a bandgap opening and suggested that the obtained nanomaterials can be used for the sensing of various amines with good affinity.[43] In another work, the same team demonstrated that graphene bearing substituted cyclopropane moieties with electron-donating groups (MeO_2C-, HO_2C-, NaO_2C- and PhCO−) are good candidates to selectively sense Pb^{2+} in presence of Cd^{2+} and Hg^{2+} in aqueous media, with predicted order of interaction of cations in agreement with experimental data.[26] Functionalized graphene with cations generated from the decomposition of p-substituted diazonium salts can be used for the detection of ammonia.[49] Kumar and Ghosh modified reduced graphene oxide with rose Bengal dye to build chemoresistive gas sensors for ammonia, ethanol and acetone.[50] In a last example, porphyrins and phthalocyanines coordinated with different metal ions [Co(II),[51] Cu(II)[52] and Zn(II)[53] were also used for ammonia sensing with good selectivity in presence of other gases such as CO_2, SO_2, NO_2, H_2S, etc.

To make progress in the field, herein we report on the use of dispersion-corrected density functional theory (DFT−D3) to investigate the modification of graphene nanosheets with substituted carbenes to obtain the corresponding carbene-functionalized graphene nanomaterials (**g7 × 7/1a−d**) that can be used as gas sensors for short chain nitrogenated compounds. We find that the modified materials can selectively sense the amines, via hydrogen-bonding interactions having energies varying from −0.5 to −0.6 eV. Additionally, we show that in the presence of water molecules the carboxylic moiety can protonate ammonia giving rise to ion pairs. Changes in electronic density, Löwdin partial charges, and projected density of states in the absence of acidic amine protonation reveal that the strongest interaction occurred between the −OH from the carboxylic group and the nitrogen atom of the amines. To investigate the selectivity of this phenomenon, we examined the interaction of **g7 × 7/1a** with other gases such as CO_2, SO_2, H_2S, and CH_4. Recovery time values estimated from adsorption energetics suggest that these nanomaterials can be used to detect nitrogenated compounds at relatively low temperatures (298 and 373 K). Importantly, we perform transmission calculations of prototypical systems based on NH_3 interacting with various functionalizers containing carboxylic moieties, both dissociated and un-dissociated, and showed that **g7 × 7** and **g7 × 7/1a** behave differently in the presence of ammonia, which should be experimentally detectable and make these materials good candidates to design sensors for ammonia.

2. COMPUTATIONAL DETAILS

Structure relaxation and band structure calculations were carried out at DFT/PBE level[54,55] with the DFT-D3 dispersion correction[56−58] implemented within the Quantum ESPRESSO (v7.0) package.[59] Valence and core electrons were expressed in terms of a discrete plane-wave basis set (cut-off = 49.15 Ry) and PAW formalism, respectively.[60,61] The conductance of the different systems was obtained by mean of the non-equilibrium green function (NEGF) approach[62] implemented within the SIESTA code,[63,64] by using double zeta plus polarization (DZP) basis set for describing the valence electrons and Hamann norm-conserving pseudopotentials for describing the inner charges.[65,66]

For all the thermodynamics and sensing simulations, we used a graphene supercell consisting of large 7 × 7 unit cells (98 carbon atoms) onto which the different organic functionalizers were chemically bound. Such a large cell was chosen to achieve a low surface coverage and avoid lateral interaction between the functionalizing groups. During the relaxation of the structures (until the maximum force on ions is less than 1×10^{-3} eV·Å^{-1}), we used a Monkhorst−Pack *k*-point grid (3 × 3 × 1) to sample the Brillouin zone and the orbital energies were broadened using Gaussian smearing of 0.01 eV. A denser Monkhorst−Pack *k*-point grid (12 × 12 × 1) and tetrahedron integration method were applied for calculating the electronic properties.

For the conductance calculations, we used graphene layers made by 120 carbon atoms laid on the basal plane of an orthorhombic unit cell (36.9 × 8.52 × 25.0 Å^3). The transmission direction, which coincides with the longest edge, also coincides with the zig-zag direction of the graphene layer.[67] We accounted for the system periodicity in the direction perpendicular to the transmission one, by employing Born−von Karman boundary conditions that allow wave vectors *K* belonging to a 100 × 1 Monkhorst−Pack regular grid. Prior to the conductance calculations, the geometry of the functionalized nanoribbons was relaxed until the maximum force on ions is less than 1×10^{-3} eV·Å^{-1} and the electronic energy is less than 1×10^{-6} Ry employing the CP2K software[68] at DFT-D3/PBE level using DZVP-Molopt-GTH basis sets[69] and GTH-PBE pseudopotentials.[70]

Cycloaddition reaction energies, ΔE_{rnx}, were determined from the difference of the individual energies of the modified graphene (E_{mg}), the carbene adsorbate ($E_{carbene}$), and the graphene ($E_{graphene}$) using eq 1.[26,43]

$$\Delta E_{rxn} = E_{mg} - (E_{graphene} + E_{carbene}) \quad (1)$$

Adsorption energy values, ΔE_{ads}, were determined from the difference of the complex energy ($E_{complex}$), the modified graphene energy (E_{mg}), and the target energy (E_{target}) using eq 2, where *n* is the number of adsorbates per supercell.[26,43]

$$\Delta E_{ads} = E_{complex} - (E_{mg} + E_{target})/n \quad (2)$$

Differences in the charge density, $\Delta\rho$, were determined from the difference of the electronic densities of the complex ($\rho_{complex}$), the modified graphene (ρ_{mg}), and the target (ρ_{target}) using eq 3.[26,43]

$$\Delta\rho = \rho_{complex} - (\rho_{mg} + \rho_{target}) \quad (3)$$

Partial charges were calculated using the Löwdin population analysis using eq 4.[26,43]

https://doi.org/10.1021/acs.jpcc.3c01945
J. Phys. Chem. C 2023, 127, 15474−15485

$$\text{Partial charge} = ne_{\text{cal.}} - ne_{\text{val.}} \quad (4)$$

where $ne_{\text{cal.}}$ and $ne_{\text{val.}}$ represent respectively the population calculated for a given atom and its number of valence electrons (H = 1.00, C = 6.00, N = 7.00, O = 8.00 and F = 9.0). The partial charge is considered negative if the calculated Löwdin electron population[71] is higher than the number of valence electrons, otherwise it is considered as positive.

Recovery times were calculated from transition-state theory according to eq 5.[72]

$$\tau = \nu^{-1} \exp(|\Delta E_{\text{ads}}|/k_{\text{b}}T) \quad (5)$$

where ν is the attempt frequency of bond breaking ($\nu \approx 1$ THz), ΔE_{ads} is the adsorbate/modified graphene interaction energy, k_{b} is the Boltzmann constant, and T is the system working temperature.

3. RESULTS AND DISCUSSION

3.1. Thermodynamics of the Graphene Functionalization. We first examined the [1 + 2]−cycloaddition reaction between the carbenes (**1a**−**d**) with the graphene (Figure 1A),

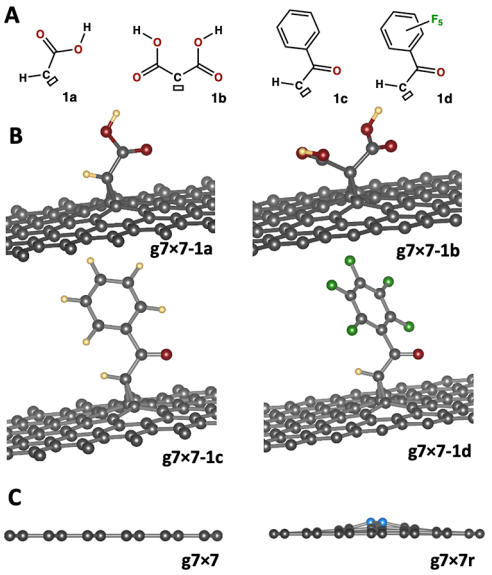

Figure 1. (A) Chemical structures of the different carbene reactive intermediates used to functionalize the graphene nanosheets, (B) 2D representation of the modified graphene nanosheets (**g7 × 7/1a**−**d**), and (C) lateral view of the flat (**g7 × 7**) and rippled (**g7 × 7r**) graphene substrates. Color code: C: black (or cyan blue), O: dark red, H: yellow, and F: green.

which yields the corresponding cyclopropane functionalized graphene nanosheets (**g7 × 7/1a**−**d**) as depicted in Figure 1B. These substituted prototypical carbenes were chosen to grasp the effects of: (i) introducing a second carboxyl substituent on the low-valence carbon atom, (ii) substituting the carboxyl group with a phenylcarboxyl group, and (iii) replacing the hydrogen atoms on the phenyl group by strong electron attracting fluorine atoms.

Data summarized in Table 1 show that the cycloaddition reaction between the graphene (**g7 × 7**) and the substituted carbenes is favorable since the reaction energy varies from −1.57 to −2.68 eV (−151.5 to −258.6 kJ·mol^{-1}). These values agree well with the data for cycloaddition reaction occurring between dienes and dienophiles.[73,74] Differences can be attributed to the electronic and steric effects caused by the different groups, in particular the lower energy value for **1b** is due to steric hindrance.

Table 1. Reaction Energies of the Organic Functionalizers with Flat and Rippled Graphene and the Corresponding Distortion Energy

substrates	reaction energy/eV[a]	reaction energy/eV[b]	rippling energy/eV[c]
g7 × 7/1a	−2.68	−3.89	−1.21
g7 × 7/1b	−1.57	−2.93	−1.36
g7 × 7/1c	−2.42	−3.62	−1.20
g7 × 7/1d	−2.32	−3.43	−1.11

[a]Reaction energy calculated starting from the flat graphene ($E_{\text{graph,flat}}$). [b]Reaction energy calculated starting from the rippled graphene ($E_{\text{graph,rippling}}$). [c]$E_{\text{rippling}} = E_{\text{graph,rippling}} - E_{\text{graph,flat}}$.

Also, for comparison with previous works,[26,43] we examined the reaction between the rippled graphene substrate (**g7 × 7r**) and the carbenes by virtually splitting the as-formed cyclopropane into a carbene group and a rippled graphene. The reaction energy values (−2.93 to −3.89 eV) are naturally higher than those computed starting from the flat graphene supercell and agree well with those reported by Hildebrand et al.[27] The differences, varying from 1.11 to 1.36 eV depending on the substituent on the low valence carbon atom, measure the energy needed for distorting the graphene (the rippling energy) by pulling out the two carbon atoms, site of the reaction, from the graphene plane and changing their hybridization from sp^2 to sp^3. These values are also consistent with the literature.[75]

3.2. Geometrical Features. Since the chemical reaction involves carbon atoms from the graphene surface, we examined the changes occurring in their geometrical features. The sp^3−sp^3 C−C bond length from the cyclopropane is longer than the simple carbon−carbon bond length in the graphene (1.57 vs 1.44 Å) and ∠CCC of 60°, which agree with values from literature.[26,31,43] Besides, the same reaction induced localized changes in the graphene structure, the involved atoms show a protrusion (0.6 to 0.7 Å) above the graphene median surface, which completely disappeared at the unit cell edges.

3.3. Electronic Properties of the Substituted Graphene. We further examined the changes induced by the organic functionalization on the graphene electronic properties. Plots of the total DOS display a transition from a system without a bandgap, suggesting a semi-metallic behavior, to a pseudo-semiconducting one with the appearance of a gap near the Fermi level (Figure 2A−D). A more precise picture is derived from the band structure plots (Figure 2E−H) showing a direct bandgap near the K point of ≈0.2 eV (note also the inflection shape in the lowest unoccupied band at the K point). Importantly, it is to be noted that the Dirac point is shifted away in K-space from the Fermi level, and, in the **1b**−**1d** cases, lies in the middle of the pseudo-bandgap (above the Fermi level). In other words, the presence of the functionalizer with the transformation of some aromatic into aliphatic carbon destroys conjugation and creates an electronic band gap in its neighborhood, whereas the graphene away from the functionalizer basically maintains its conducting electronic structure. This explain the band gap at the K point, and the shift of the Dirac point to another position of the Brillouin zone. Previous Results on similar systems in previous literature

https://doi.org/10.1021/acs.jpcc.3c01945
J. Phys. Chem. C 2023, 127, 15474−15485

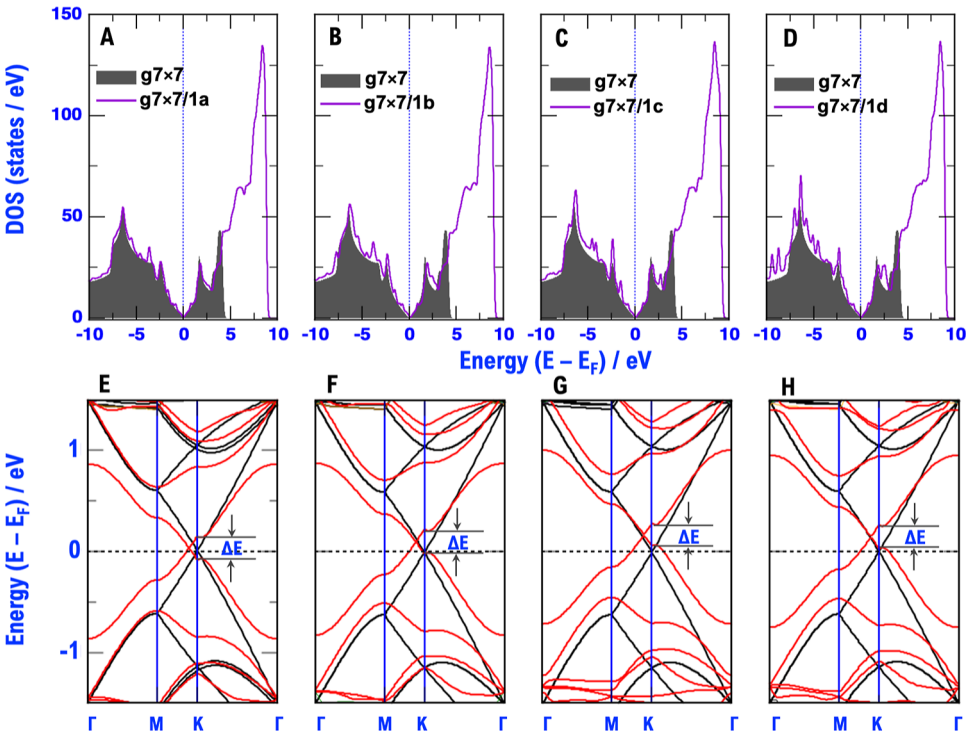

Figure 2. Plots of the total DOS (A–D) where the grey plain plots are for the pristine graphene and the violet plots are for the corresponding functionalized graphene. Band structures (E–H) for the different carbene-functionalized graphene nanosheets **g7 × 7/1a–d** showing the band gap opening at the *K*-point. The black plots are for the unmodified graphene and are given for comparison.

are consistent with the more detailed picture here presented.[26,43]

3.4. Detection of Volatile Amines. Next, we investigated the sensing capability of the functionalized graphene derivatives (**g7 × 7/1a–d**) to detect ammonia and other short-chain volatile amines (MMA, DMA, and TMA). Adsorption energy was calculated from the energies of the complex, the modified graphene, and the adsorbate (target), according to eq 2. Data gathered in Table 2 show that the nitrogenated derivatives interact favorably with the different carbene-functionalized graphene derivatives. The highest energy values (−0.49 to −0.60 eV) were observed with the amines, which can be attributed to the strong hydrogen bond (HB) between the OH from the CO_2H group and the nitrogen from the amines. Additionally, we examined the potential ability of **g7 × 7/1b** to sense more than one molecule of amine. Structural relaxation of the modified graphene in the presence of two NH_3, MMA, DMA, or TMA showed that the energy values are almost twice larger than those obtained with one molecule of the target amine, which agrees with the fact the substrate is involved in HB using both carboxylic groups with the two amines. Additionally, the adsorption energies per one adsorbate molecule are almost the same as that computed for one target, denoting a decoupled adsorption. In our study, we intentionally used a low surface coverage of the organic functionalized (one carbene group for every 100 graphene carbon atoms). One can expect that increasing the surface coverage (one carbene group every 40 to 50 graphene carbons in smaller supercells) will allow detecting a higher number of the targets and thus reaching a higher sensitivity.

Furthermore, the interaction energies for the derivatives bearing the carboxylic acid group (**g7 × 7/1a–b**) are higher than those computed with the ketone substituents. This was expected since the carboxylic acid groups act as strong hydrogen bonding donors than the ketone with the nitrogen atom of the amines as hydrogen acceptors, while the NH···CO hydrogen bonds are weaker. We can observe that the interaction energy values between the amines and **g7 × 7/1d** are lower than that with **g7 × 7/1c** because the strong electronic withdrawing effect of fluorine atoms in **g7 × 7/1d** weakens the C═O group hydrogen bond accepting behavior.

It is worth noting that the DFT/PBE typically somewhat overestimates the interaction energy between the acidic group of the formic acid and the ammonia target.[76] Indeed, in Table S1 of the Supporting Information we report the results of the comparison among interaction energies computed according to different methods, showing that depending on the method the increase in energy may range from 20 to 290 meV. We also note however that it is difficult to reach high accuracy on this quantity: even computationally expensive post-Hartree–Fock CCSDT/DZ and M08-HX methods overestimate the interaction energy by 17.5 and 6.4%, respectively, when compared to the CCSDT/QVZ method, which we report and is believed to achieve chemical accuracy. Despite these limitations, PBE/D3 is the only computationally affordable method to investigate the large unit cells of the present study.

3.5. Electron Density Differences. To gain further insight into the changes in the electronic density distribution after the interaction with the target and potentially interfering molecules, we computed the charge density difference using eq 3. Panel A of Figure 3 displays the charge variations after interaction with NH_3, MMA, DMA, and TMA. The charge density plots show area of charge depletion (colored in blue) around the hydrogen and oxygen atoms of the carboxylic acid group along with areas of charge gain (colored in yellow) in the vicinity of the nitrogen. We attribute this to a charge

https://doi.org/10.1021/acs.jpcc.3c01945
J. Phys. Chem. C 2023, 127, 15474–15485

Table 2. Calculated Adsorption Energy of the Nitrogenated Compounds with the Different Modified Graphene Nanosheets (g7 × 7/1a−1d), HB Donors and Acceptors Involved in the HB and Their Lengths

substrates	targets	ΔE_{ads} (eV)	involved atoms	d (Å)
g7 × 7/1a	NH_3	−0.49	OH···N	1.66 (2.95)[a]
	MMA	−0.52	OH···N	1.63 (2.65)[a]
	DMA	−0.55	OH···N	1.60 (2.95)[a]
	TMA	−0.51	OH···N	1.62
g7 × 7/1a	Cl_2	−0.18	OH···Cl	2.41
	H_2S	−0.18	OH···S	2.39
	CO_2	−0.08	OH···O	2.12
	SO_2	−0.02	OH···S	3.02
g7 × 7/1b	NH_3	−0.56	OH···N/C═O···HN	1.63 (2.51)[a]
	MMA	−0.57	OH···N/C═O···HN	1.58 (2.86)[a]
	DMA	−0.58	OH···N/C═O···HN	1.54 (2.41)[a]
	TMA	−0.50	OH···N	1.56
g7 × 7/1b	$2NH_3$	−0.58	OH···N	1.64 (1.65)[b,c]
	2MMA	−0.63	OH···N	1.59 (1.60)[b,c]
	2DMA	−0.60	OH···N	1.54 (1.57)[b,c]
	2TMA	−0.61	OH···N	1.53 (1.56)[b,c]
g7 × 7/1c	NH_3	−0.11	C═O···HN	16
	MMA	−0.12	C═O···HN	2.20
	DMA	−0.13	C═O···HN	2.14
	TMA	−0.04	C═O···HC	3.12[d]
g7 × 7/1d	NH_3	−0.05	C═O···HN	2.22
	MMA	−0.08	C═O···HN	2.25
	DMA	−0.10	C═O···HN	2.39
	TMA	−0.01	C═O···HC	2.82[d]

[a]The target established a second nonlinear HB between the C═O group and NH from the amine. [b]Length of the second OH···N hydrogen bond. [c]Each OH group established an HB with the target molecule. [d]Weak CH···OC hydrogen bond.

density redistribution following the hydrogen bond formation. All the carbons of the graphene substrate and the carbene are unaffected by the interaction and their electronic density remained unchanged.

3.6. Selectivity. To examine the selectivity of the modified graphene surface toward the nitrogenated target molecules, we calculated the interaction of the prototypical **g7 × 7/1a** with other gases such as Cl_2, CO_2, H_2S, and SO_2. Table 2 (entry 2) and panel B of Figure 3 report the corresponding results of charge density differences. From the data, we remark that the interaction of these competing species is generally weaker, meaning that sensing will be selective towards amines. The interaction energy does not exceed −0.20 eV, which the one-third of the lowest energy computed for CO_2H···NR_3 (R = H, CH_3) systems, thus demonstrating a good selectivity of the surface toward amines, thanks to the high hydrogen bonding donating ability. Carbon dioxide and sulfur dioxide seem to be the least attracted to the surface because of the lone pairs of electrons on the oxygens, which probably are causing repulsion with the oxygen-rich group tethered to the graphene surface. Also, as expected, the areas of charge gains and losses in panel B of Figure 3 are more sizeable with the chlorine and H_2S molecules than with CO_2 and SO_2. In all cases, the charge density differences with the competing gases are weaker than with those obtained for the amines (note that panels A and B are represented using two different isovalues of the charge density).

3.7. Projected Density of States. To further analyze the amine/functionalized-graphene interaction, we calculated the PDOS for the atoms of the two groups involved in the interaction (H_3N and the carboxylic acid), and other carbon atoms from the carbene functionalizer and one carbon in the graphene far from the reaction center. In panel A of Figure 4, we can observe a shift by 2.1 and 0.3 eV to lower energy values of the orbital energy of the N_{2p} and the H_{1s} after adsorption, respectively. Also, the 2p orbitals of the two oxygens of the carboxylic acid are shifted to lower energy after adsorption. The extent of the shift is weaker (0.4 eV), which suggests that the influence of the interaction weakens far from the reaction center. The 2p orbitals of the C(sp^2) atom of the carboxylic acid are shifted to higher energy values by 0.6 eV after the interaction (black plot), while the CH group of the carbene is influenced to a lesser extent (red plot) and the other carbons

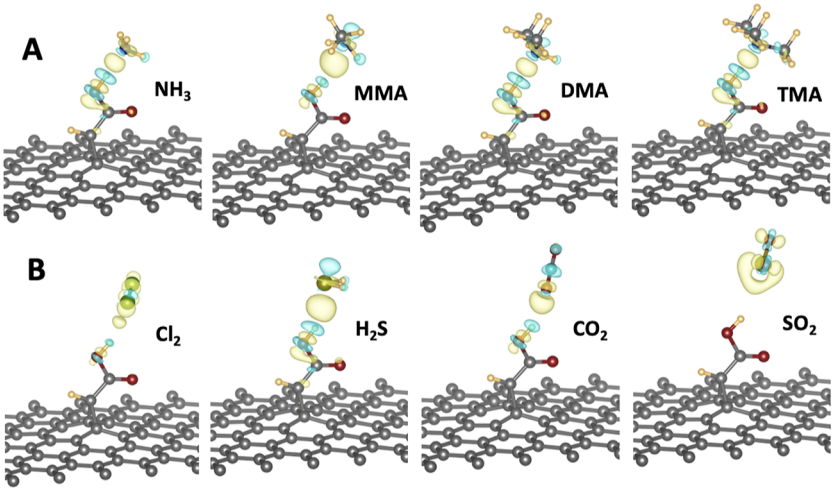

Figure 3. (A) Selected optimized geometries of cyclopropane-modified graphene derivatives **g7 × 7/1a** in interaction with NH_3, MMA, DMA, and TMA molecules. (B) Modified graphene substrate interaction with Cl_2, H_2S, CO_2, and SO_2 molecules. Isovalues of the charge density difference were set at 1.0×10^{-3} e·bohr^{-3} (A) and 3.0×10^{-3} e·bohr^{-3} (B).

https://doi.org/10.1021/acs.jpcc.3c01945
J. Phys. Chem. C 2023, 127, 15474−15485

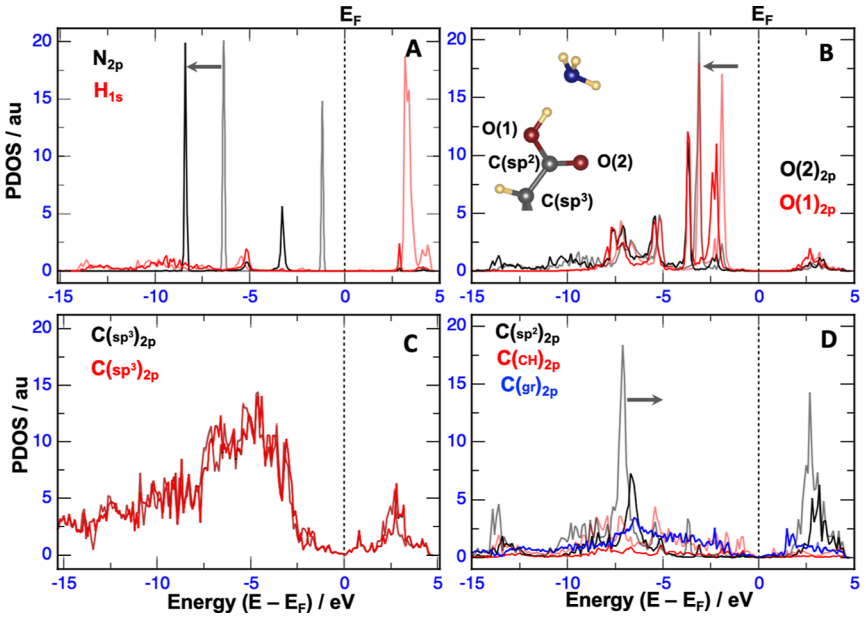

Figure 4. PDOS of the atoms involved in the interactions: (A) H_{1s} from the acidic group and N_{2p} form the ammonia, (B) 2p orbitals of the two oxygens from the carboxylic acid, (C) 2p orbitals of the two carbons involved in the cycloaddition and (D) 2p orbitals of the sp^2 carbon from the carboxylic acid, from the CH group and a random carbon from the graphene surface far from the reaction center.

of the graphene are unaffected (blue plot in panel D). The projected DOS of C−C atoms siege of the cycloaddition reaction shows no influence of the interaction on their energy levels, thus confirming the effect of the distance (panel C).

3.8. Partial Charges. The computed partial charges from the Löwdin population analysis changed after adsorption (Figure 5). It is worth noticing that the variation in the electronic charge is proportional to the extent of the interaction between the substrate and the target, as depicted in Figure 5A,B. In the case of the interaction between **g7 × 7/1a** and ammonia, the highest partial charge changes occur in the vicinity of the interaction center, where the nitrogen loses charge density (−0.09*e*) and draws electrons from the three adjacent hydrogens, on which the partial charge increases by +0.08*e*. The acidic hydrogen also loses charge density (−0.05*e*) upon adsorption, by gaining charge density from the two oxygens. The partial charges of the latter and the sp^2-carbon from the carboxylic acid witness weaker gains in their partial charges (+0.03*e*), due to a longer distance separating them from the hydrogen bond location. The CH group shows almost no partial charge change (loss of 0.01*e*), thus demonstrating the proximity of these charge effects to the interaction center.

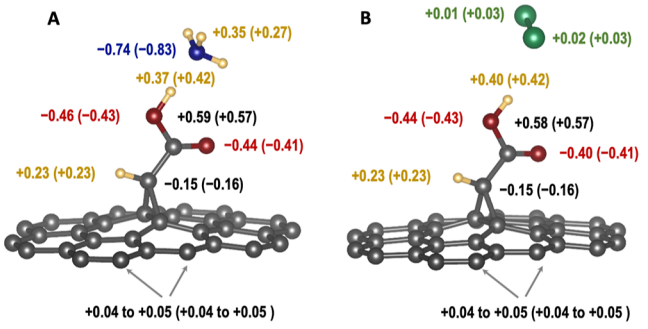

Figure 5. Computed partial charges before between brackets and after the interaction of **g7 × 7/1a** with ammonia (A) and chlorine (B). Atoms of the graphene were removed for clarity.

In the case of the interaction between **g7 × 7/1a** and Cl_2, the overall trend is similar to those observed in the interaction between **g7 × 7/1a** and ammonia but they are appreciably weaker. For instance, the chlorine charge distribution is only slightly disturbed by the interaction and the acidic proton only loses −0.02*e* following the interaction. Additionally, the partial charges of the graphene substrate seem to be unaffected by the interaction. The overall partial charge variation does not

Table 3. Recovery Times Calculated at 298 and at 373 K for the Different g7 × 7/1a−b in the Presence of the Amines and the Potential Interfering Targets

g7 × 7/1a			g7 × 7/1b		
target	recovery time (298 K)/μs	recovery time (373 K)/μs	target	recovery time (298 K)/μs	recovery time (373 K)/μs
NH_3	194	4	NH_3	2956 (6440)	37 (68)
MMA	623	11	MMA	4363 (45,131)	50 (325)
DMA	2002	27	DMA	6440 (14,032)	68 (128)
TMA	422	8	TMA	286 (20,713)	6 (174)
Cl_2	1.1×10^{-3}	0.3×10^{-3}			
CO_2	1.1×10^{-6}	0.3×10^{-6}			

https://doi.org/10.1021/acs.jpcc.3c01945
J. Phys. Chem. C 2023, 127, 15474−15485

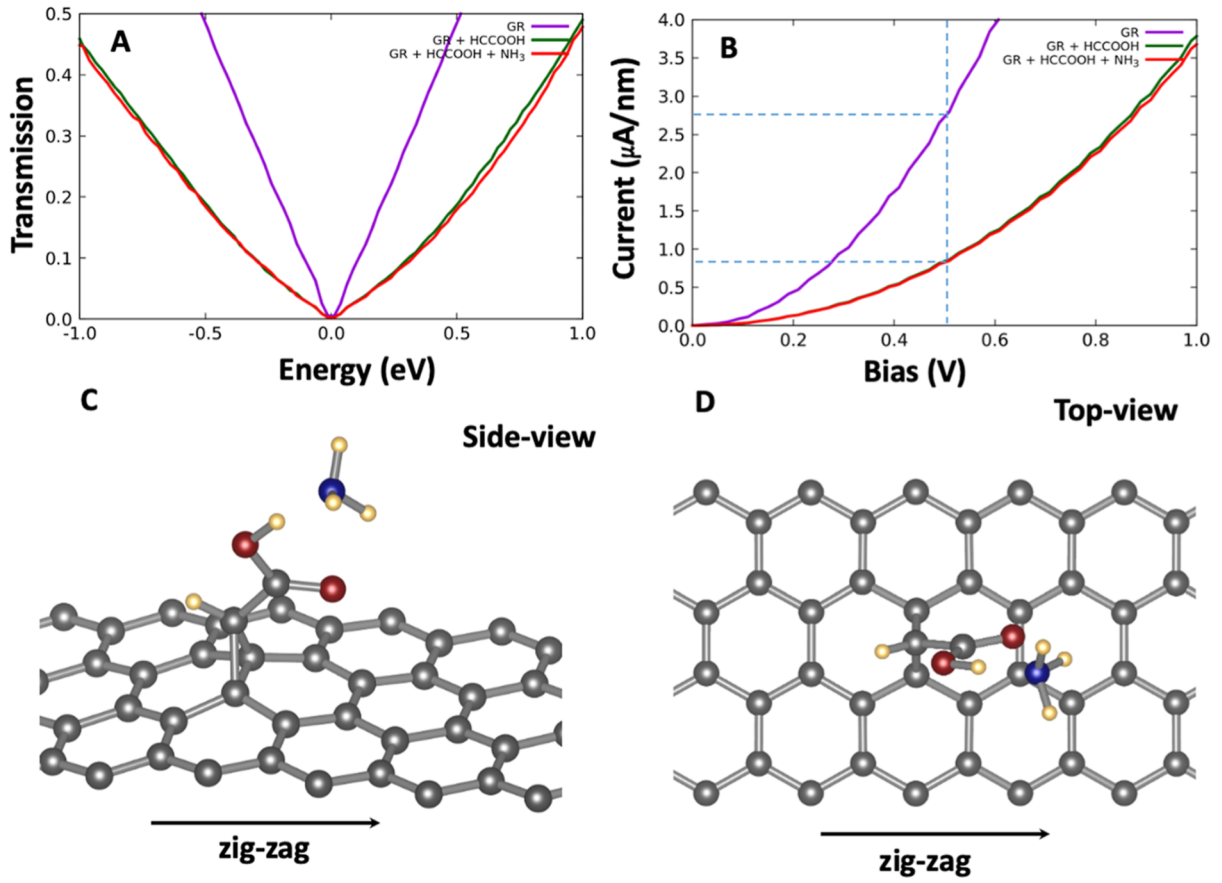

Figure 6. Panel (A) Electronic transmission plots at different energies for the bare graphene (violet) and the **g7 × 7/1a** nanosheet with (red) and without (green) ammonia. Panel (B) Simulated current density under different potential biases for the bare graphene (violet) and the **g7 × 7/1a** nanosheet with (red) and without (green) ammonia. Panels (C,D) contain different views of ball and stick representations of the functionalized graphene layer in interaction with the ammonia molecule.

exceed 0.02*e* arising from the weak interaction between the target and the substituted graphene.

3.9. Recovery Time. To assess the potential use of these nanomaterials in the detection of the nitrogenated compounds, we determined the recovery times at ambient temperature (298 K) and at 373 K, using eq 5. The data are gathered in Table 3.

Assuming a reasonable Arrhenius prefactor and at ambient temperature, the recovery time values for the modified graphene **g7 × 7/1a** and **g7 × 7/1b** were calculated. The values span from 0.2 to 2.0 ms and from 0.3 to 45.1 ms, respectively. At 373 K, the time values are two to 3 orders of magnitude lower and range from 4 to 27 μs and 6 to 325 μs. It is worth noticing that the millisecond to microsecond time scale is shorter than the times required to realize detection in an experimental setup since the device cannot hold the gas molecules for times long enough to be detected by the electronic circuit.[8,9] On the other hand, all the examined interfering gases have a weak interaction with the surface except Cl_2 and H_2S. The recovery time values of the latter are in the nanosecond range, which does not qualify the investigated materials sensors to detect these species in a real experimental setup. This is attributed to the weak interaction energies (<−0.2 eV) recorded for the carbene-functionalized graphene nanosheets. Although, the huge differences in recovery times show that the nanomaterials can be used selectively to detect the aminated compounds in the presence of CO_2, SO_2, Cl_2, and H_2S if the interaction energy can be enhanced by increasing the density of the detection sites.

3.10. Conductance and Integrated Currents. The above band structure and wave function analysis provide useful insights into the interaction between functionalized graphene and amines, but they are not sufficient to demonstrate the feasibility of using this system in sensing. To demonstrate this, we must prove that some property of the system, accessible to experimental measurement, is affected by the formation of the target−substrate complex in a degree sufficient to be detected in practice.[77−80] The property of choice in the case of graphene is conductance. We, therefore, investigated how conductance changes as a function of amine interaction via first-principles electronic transport simulations. First, we calculated the conductance of pristine graphene, with the transmission measured along *a* direction parallel to the zig-zag one (panels C and D of Figure 6). The results of Figure 6 show that the current flows as the potential bias increases as expected for a semi-conductive material with a zero bandgap (Figure 6, GR curve in purple) and in this respect are consistent with similar simulations reported in the literature (see e.g. ref 81). Differently from previous cases, we find that the current density, which is *ca.* 0.025 $\mu A \cdot nm^{-1}$ at a potential bias of 50 mV, drastically increases by about 2 orders of magnitude (2.70 $\mu A \cdot nm^{-1}$) when the applied potential bias increased 10 times, implying a nonlinear behavior. In the case of functionalized graphene (**g7 × 7/1a**), the calculated current shows an overall similar behavior since the current increases

https://doi.org/10.1021/acs.jpcc.3c01945
J. Phys. Chem. C 2023, 127, 15474−15485

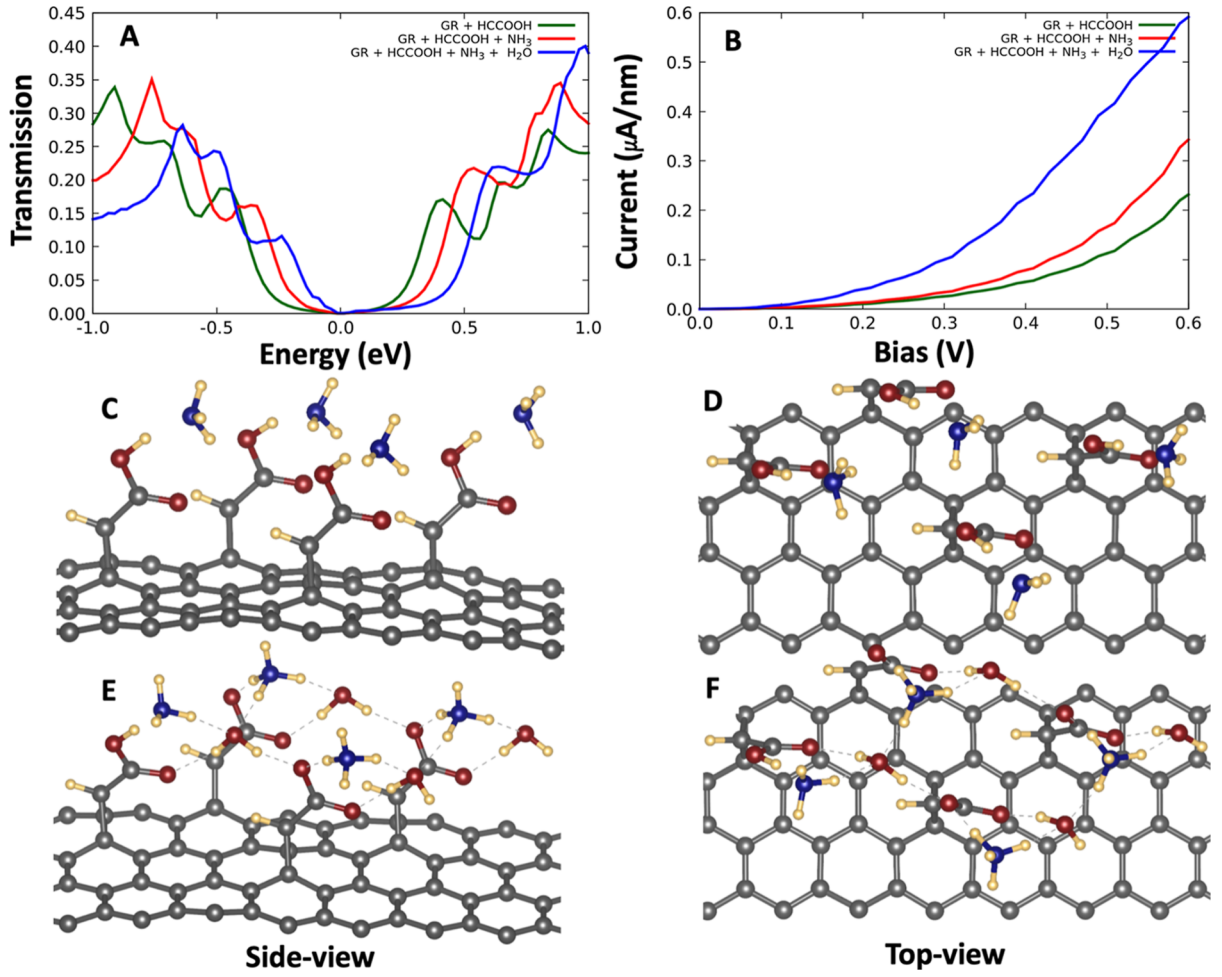

Figure 7. Panel (A) Electronic transmission plots at different energies for the bare (green) **g7 × 7/1a** nanosheet in the presence of ammonia (red) and after the addition of one water molecule per carboxylic acid function (blue). Panel (B) simulated current density under different potential biases for the bare (green) **g7 × 7/1a** nanosheet in the presence of ammonia (red) and after the addition of water (blue). Panels (C,D) contain different views of ball and stick representations of the functionalized graphene layer in interaction with the ammonia molecule. Panels (E,F) contain different views of ball and stick representations of the functionalized graphene layer in interaction with the ammonia molecule after the addition of water molecules. Dashed lines represent the hydrogen bond network established on the surface of the modified graphene by the carboxylate ion, the ammonium ion, and the water molecules.

concomitantly with the potential bias increase (Figure 6 green curve). However, the recorded maximum current is ca. 70% lower than that recorded for the pristine graphene. Indeed, for a potential bias of 0.5 V, the currents are respectively 2.70 and 0.85 $\mu A \cdot nm^{-1}$ for the pristine and modified graphene. We therefore conclude that the covalently bounded carbene unit is able to reduce the electronic states available for charge transport along the transmission direction even at a density as low as 1 group per 120 graphene carbons (about 0.5 $pmol \cdot mm^{-2}$), see Figure 6 panel C for an atomistic depiction of the system.

On the contrary, by considering the system illustrated in Figure 6 panel D, we find that, under these conditions, the ammonia presence (Figure 6, panel B, red curve) hardly affects the functionalized graphene's current response, which is reduced by only about 3% when the bias is 1.0 V. We attribute this unexpected low sensitivity to both the low density of interaction sites and especially to a relatively low interaction between the ammonia and the acid moiety, which do not generate a surface dipole strong enough to appreciably modify the electronic states and thus the transmission of the functionalized graphene along the considered direction. In other words, the number of conductance paths affected by the presence of ammonia is small and has little effect on the current. We thus explored the effect of a larger density of carbene groups on the electronic current, to see whether this can induce a larger and more uniform dipole in the direction transverse to transmission. To do this, we added three more HC−CO_2H groups (**1a**) surrounding the initial one within a stripe of graphene about 10 Å width (Figure 7, panels C and D).

The results of the current simulations (Figure 7, panels A and B) indicate, first, that the carbene density increasing drastically modifies both the shape and the intensity of transmission, which loses the characteristic V configuration and reduces almost linearly with the number of carbene units. The higher carbene coverage also improves the functionalized graphene sensitivity in detecting ammonia presence, since the larger and more uniform dipole, generated from the interactions of the amines with the CO_2H groups, destabilizes the electronic states of the graphene responsible for conductance that now passes directly underneath the adsorbed amine and increases their density near the Fermi level, leading to an improved transmission at low bias (Figure 7, panel A red

https://doi.org/10.1021/acs.jpcc.3c01945
J. Phys. Chem. C 2023, 127, 15474−15485

curve) and a current density larger by about 50% at 0.6 V (Figure 7, panel B red curve) than the one recorded in the same condition for functionalized graphene in the absence of amine (Figure 7, panel B green curve). This phenomenon is akin to the one previously investigated for graphene/electrode interfaces[81] and could be similarly rationalized by comparing the electrostatic potential profile of the bare and amine-interacting graphene systems. This degree of change of the current density with ammonia presence (around 50% difference in the signal) should be sufficient to be experimentally detectable, as the current state of the art in sensor devices presents a $1/f$ noise level ranging between 5 and 50% depending on device configuration.[82] Furthermore, the strength of the surface dipole and consequently the intensity of the current density can be further increased by the addition of water with a concentration similar to that of ammonia (Figure 7 panel D and E). In this case, in fact, our simulations predict the formation of ion pairs NH_4^+/CO_2^- following proton transfer from the acid group to ammonia. The proton transfer is critically promoted by the water molecules that stabilize the negative charge left on the carboxylic groups from the transferred proton leading to the formation of ammonium ions. NH_4^+/CO_2^- and water molecules established a dense network of hydrogen bonds stabilizing the charge on the surface (as shown in Figure 7), which increases the electronic effects. As shown from the data reported in panel B of Figure 7, the formation of ion pairs increases the current density of the functionalized graphene by about 270%, suggesting a combined sensing of ammonia and water, or in general a dependence on ammonia detection by this sensing system upon humidity.

4. CONCLUSIONS

The functionalization of graphene with reactive groups with tailored properties is of paramount importance in the field of materials research aimed at developing sensors for the detection of ammonia, in order to assess low levels of contaminants that can endanger public safety. Using DFT, we showed that graphene can be modified by carbenes to yield corresponding functionalized graphene nanomaterials *via* a cycloaddition reaction, with reaction energy varying from −1.6 to −2.9 eV, where these energies are reduced by the energy lost to deform graphene (−1.1 to −1.4 eV). These nanomaterials can interact with nitrogenated compounds *via* hydrogen bonding with sizeable interaction energies ranging from −0.5 to −0.6 eV. The mechanism of interaction was analyzed using PDOS, partial charges, and differences of charge density, providing a consistent physicochemical picture. The predicted short recovery times and selectivity towards amines rather than possible competing adsorbates (CO_2, SO_2, Cl_2, and H_2S) indicate that the materials here investigated could offer a possible pathway to design electronic field-effect transistors for the detection of amine derivatives in complex gaseous samples. This is demonstrated by complementing static calculations with novel first-principles explicit simulations of electronic transport (i−v curves), illustrating under which conditions the presence of interacting amines can affect conductance to a degree which can be experimentally measured.

ASSOCIATED CONTENT

Supporting Information

The Supporting Information is available free of charge at https://pubs.acs.org/doi/10.1021/acs.jpcc.3c01945.

Phonon spectra of unmodified and modified graphene; interaction energies computed for formic acid/ammonia (PDF)

AUTHOR INFORMATION

Corresponding Authors

Alessandro Fortunelli − *Consiglio Nazionale delle Ricerche, CNR−ICCOM & IPCF, Pisa 56124, Italy*; orcid.org/0000-0001-5337-4450; Email: alessandro.fortunelli@cnr.it

Adnene Dhouib − *Department of Chemistry, College of Science, Imam Abdulrahman Bin Faisal University, Dammam 31113, Saudi Arabia*; Email: amdhouib@iau.edu.sa

Noureddine Raouafi − *Laboratory of Analytical Chemistry and Electrochemistry (LR99ES15), Chemistry Department, Faculty of Science of Tunis, University of Tunis El Manar, Tunis El Manar 2092, Tunisia*; orcid.org/0000-0001-8938-8221; Email: noureddine.raouafi@fst.utm.tn

Authors

Sabrine Baachaoui − *Laboratory of Analytical Chemistry and Electrochemistry (LR99ES15), Chemistry Department, Faculty of Science of Tunis, University of Tunis El Manar, Tunis El Manar 2092, Tunisia*; orcid.org/0000-0003-0972-6484

Luca Sementa − *Consiglio Nazionale delle Ricerche, CNR−ICCOM & IPCF, Pisa 56124, Italy*

Rabiaa Hajlaoui − *Laboratory of Analytical Chemistry and Electrochemistry (LR99ES15), Chemistry Department, Faculty of Science of Tunis, University of Tunis El Manar, Tunis El Manar 2092, Tunisia*

Sarah Aldulaijan − *Department of Chemistry, College of Science, Imam Abdulrahman Bin Faisal University, Dammam 31113, Saudi Arabia*

Complete contact information is available at: https://pubs.acs.org/10.1021/acs.jpcc.3c01945

Author Contributions

S.B. and L.S. contributed equally. SB: Investigation and data curation, LS: investigation, validation, supervision, writing—review & editing, RB, investigation and data curation, SA: investigation and data curation, AF: validation, supervision, writing—review & editing, AD: validation, funding acquisition, NR: methodology, supervision, validation, writing—review & editing.

Notes

The authors declare no competing financial interest.

ACKNOWLEDGMENTS

For computer time, this research (project ref. k1396) used the resources of the Supercomputing Laboratory at King Abdullah University of Science & Technology (KAUST) in Thuwal, Saudi Arabia.

REFERENCES

(1) Ojelade, O. A.; Zaman, S. F.; Ni, B. J. Green ammonia production technologies: A review of practical progress. *J. Environ. Manage.* **2023**, *342*, 118348.

(2) Yüzbaşıoğlu, A. E.; Avşar, C.; Gezerman, A. O. The current situation in the use of ammonia as a sustainable energy source and its industrial potential. *Curr. Res. Green Sustainable Chem.* **2022**, *5*, 100307.

(3) Guerra, F. D.; Smith Jr, G. D.; Alexis, F.; Whitehead, D. C. A Survey of VOC Emissions from Rendering Plants. *Aerosol Air Qual. Res.* **2017**, *17*, 209−217.
(4) Phillips, V. R.; Scholtens, R.; Lee, D.; Garland, J. A.; Sneath, R. W. SE—Structures and Environment: A Review of Methods for Measuring Emission Rates of Ammonia from Livestock Buildings and Slurry or Manure Stores, Part 1: Assessment of Basic Approaches. *J. Agric. Eng. Res.* **2000**, *77*, 355−364.
(5) Sato, M. Fish inspection. In *Encyclopedia of Meat Sciences*; Jensen, W. K., Ed.; Elsevier, 2004; pp 474−483.
(6) Kroto, H. W. H.; Heath, J. R.; O'Brien, S. C.; Curl, R. F.; Smalley, R. E. C60 : Buckminsterfullerene. *Nature* **1985**, *318*, 162−163.
(7) Alzate-Carvajal, N.; Luican-Mayer, A. Functionalized Graphene Surfaces for Selective Gas Sensing. *ACS Omega* **2020**, *5*, 21320−21329.
(8) Aasi, A.; Mehdi Aghaei, S.; Panchapakesan, B. Outstanding Performance of Transition-Metal-Decorated Single-Layer Graphene-like BC6N Nanosheets for Disease Biomarker Detection in Human Breath. *ACS Omega* **2021**, *6*, 4696−4707.
(9) Mehdi Aghaei, S.; Monshi, M. M.; Torres, I.; Zeidi, S. M. J.; Calizo, I. DFT study of adsorption behavior of NO, CO, NO2, and NH3 molecules on graphene-like BC3: A search for highly sensitive molecular sensor. *Appl. Surface Sci.* **2018**, *427*, 326−333.
(10) Yue, Q.; Shao, Z.; Chang, S.; Li, J. Adsorption of gas molecules on monolayer MoS2 and effect of applied electric field. *Nanoscale Res. Lett.* **2013**, *8*, 425.
(11) Hwang, M. T.; Heiranian, M.; Kim, Y.; You, S.; Leem, J.; Taqieddin, A.; Faramarzi, V.; Jing, Y. H.; Park, I.; van der Zande, A. M.; et al. Ultrasensitive detection of nucleic acids using deformed graphene channel field effect biosensors. *Nat. Commun.* **2020**, *11*, 1543.
(12) Kuila, T.; Bose, S.; Khanra, P.; Mishra, A. K.; Kim, N. H.; Lee, J. H. Recent advances in graphene-based biosensors. *Biosens. Bioelectron.* **2011**, *26*, 4637−4648.
(13) Mars, A.; Hamami, M.; Bechnak, L.; Patra, D.; Raouafi, N. Curcumin-graphene quantum dots for dual mode sensing platform: Electrochemical and fluorescence detection of APOe4, responsible of Alzheimer's disease. *Anal. Chim. Acta* **2018**, *1036*, 141−146.
(14) Rabti, A.; Ben Aoun, S.; Raouafi, N. A sensitive nitrite sensor using an electrode consisting of reduced graphene oxide functionalized with ferrocene. *Microchim. Acta* **2016**, *183*, 3111−3117.
(15) Rabti, A.; Mayorga-Martinez, C. C.; Baptista-Pires, L.; Raouafi, N.; Merkoci, A. Ferrocene-functionalized graphene electrode for biosensing applications. *Anal. Chim. Acta* **2016**, *926*, 28−35.
(16) Rabti, A.; Argoubi, W.; Raouafi, N. Enzymatic sensing of glucose in artificial saliva using a flat electrode consisting of a nanocomposite prepared from reduced graphene oxide, chitosan, nafion and glucose oxidase. *Microchim. Acta* **2016**, *183*, 1227−1233.
(17) Zouari, M.; Campuzano, S.; Pingarrón, J. M.; Raouafi, N. Determination of miRNAs in serum of cancer patients with a label- and enzyme-free voltammetric biosensor in a single 30-min step. *Microchim. Acta* **2020**, *187*, 444−511.
(18) Bakandritsos, A.; Pykal, M.; Błoński, P.; Jakubec, P.; Chronopoulos, D. D.; Poláková, K.; Georgakilas, V.; Čépe, K.; Tomanec, O.; Ranc, V.; et al. Cyanographene and Graphene Acid: Emerging Derivatives Enabling High-Yield and Selective Functionalization of Graphene. *ACS Nano* **2017**, *11*, 2982−2991.
(19) Bakandritsos, A.; Chronopoulos, D. D.; Jakubec, P.; Pykal, M.; Čépe, K.; Steriotis, T.; Kalytchuk, S.; Petr, M.; Zbořil, R.; Otyepka, M. High-Performance Supercapacitors Based on a Zwitterionic Network of Covalently Functionalized Graphene with Iron Tetraaminophthalocyanine. *Adv. Funct. Mater.* **2018**, *28*, 1801111.
(20) Chronopoulos, D. D.; Bakandritsos, A.; Pykal, M.; Zbořil, R.; Otyepka, M. Chemistry, properties, and applications of fluorographene. *Appl. Mater. Today* **2017**, *9*, 60−70.
(21) Chronopoulos, D. D.; Medved', M.; Potsi, G.; Tomanec, O.; Scheibe, M.; Otyepka, M. Tunable one-step double functionalization of graphene based on fluorographene chemistry. *Chem. Commun.* **2020**, *56*, 1936−1939.
(22) Chronopoulos, D. D.; Medved', M.; Błoński, P.; Nováček, Z.; Jakubec, P.; Tomanec, O.; Bakandritsos, A.; Novotná, V.; Zbořil, R.; Otyepka, M. Alkynylation of graphene via the Sonogashira C−C cross-coupling reaction on fluorographene. *Chem. Commun.* **2019**, *55*, 1088−1091.
(23) Ghosh, S.; An, X.; Shah, R.; Rawat, D.; Dave, B.; Kar, S.; Talapatra, S. Effect of 1- Pyrene Carboxylic-Acid Functionalization of Graphene on Its Capacitive Energy Storage. *J. Phys. Chem. C* **2012**, *116*, 20688−20693.
(24) Zaharie-Butucel, D.; Potara, M.; Craciun, A. M.; Boukherroub, R.; Szunerits, S.; Astilean, S. Revealing the structure and functionality of graphene oxide and reduced graphene oxide/pyrene carboxylic acid interfaces by correlative spectral and imaging analysis. *Phys. Chem. Chem. Phys.* **2017**, *19*, 16038−16046.
(25) Rabti, A.; Raouafi, N.; Merkoçi, A. Bio (sensing) devices based on ferrocene−functionalized graphene and carbon nanotubes. *Carbon* **2016**, *108*, 481−514.
(26) Baachaoui, S.; Aldulaijan, S.; Sementa, L.; Fortunelli, A.; Dhouib, A.; Raouafi, N. Density Functional Theory Investigation of Graphene Functionalization with Activated Carbenes and Its Application in the Sensing of Heavy Metallic Cations. *J. Phys. Chem. C* **2021**, *125*, 26418−26428.
(27) Hildebrand, M.; Abualnaja, F.; Makwana, Z.; Harrison, N. M. Strain Engineering of Adsorbate Self-Assembly on Graphene for Band Gap Tuning. *J. Phys. Chem. C* **2019**, *123*, 4475−4482.
(28) Sainsbury, T.; Passarelli, M.; Naftaly, M.; Gnaniah, S.; Spencer, S. J.; Pollard, A. J. Covalent Carbene Functionalization of Graphene: Toward Chemical Band-Gap Manipulation. *ACS Appl. Mater. Interfaces* **2016**, *8*, 4870−4877.
(29) Lazar, P.; Chua, C. K.; Hola, K.; Zboril, R.; Otyepka, M.; Pumera, M. Dichlorocarbene-Functionalized Fluorographene: Synthesis and Reaction Mechanism. *Small* **2015**, *11*, 3790−3796.
(30) Sainsbury, T.; O'Neill, A.; Passarelli, M. K.; Seraffon, M.; Gohil, D.; Gnaniah, S.; Spencer, S. J.; Rae, A.; Coleman, J. N. Dibromocarbene Functionalization of Boron Nitride Nanosheets: Toward Band Gap Manipulation and Nanocomposite Applications. *Chem. Mater.* **2014**, *26*, 7039−7050.
(31) Zan, W. Y. Chemical functionalization of graphene by carbene cycloaddition: A density functional theory study. *Appl. Surface Sci.* **2014**, *311*, 377−383.
(32) Sarkar, S.; Bekyarova, E.; Haddon, R. C. Chemistry at the Dirac point: Diels-Alder reactivity of graphene. *Acc. Chem. Res.* **2012**, *45*, 673−682.
(33) Sarkar, S.; Bekyarova, E.; Niyogi, S.; Haddon, R. C. Diels-Alder chemistry of graphite and graphene: graphene as diene and dienophile. *J. Am. Chem. Soc.* **2011**, *133*, 3324−3327.
(34) Brisebois, P. P.; Kuss, C.; Schougaard, S. B.; Izquierdo, R.; Siaj, M. New Insights into the Diels-Alder Reaction of Graphene Oxide. *Chemistry* **2016**, *22*, 5849−5852.
(35) Boukhvalov, D. W. DFT modeling of the covalent functionalization of graphene: from ideal to realistic models. *RSC Adv.* **2013**, *3*, 7150−7159.
(36) Junkermeier, C. E.; Solenov, D.; Reinecke, T. L. Adsorption of NH2 on Graphene in the Presence of Defects and Adsorbates. *J. Phys. Chem. C* **2013**, *117*, 2793−2798.
(37) Goler, S.; Coletti, C.; Tozzini, V.; Piazza, V.; Mashoff, T.; Beltram, F.; Pellegrini, V.; Heun, S. Influence of Graphene Curvature on Hydrogen Adsorption: Toward Hydrogen Storage Devices. *J. Phys. Chem. C* **2013**, *117*, 11506−11513.
(38) Gao, M.; Pan, Y.; Huang, L.; Hu, H.; Zhang, L. Z.; Guo, H. M.; Du, S. X.; Gao, H. J. Epitaxial growth and structural property of graphene on Pt(111). *Appl. Phys. Lett.* **2011**, *98*, 033101.
(39) Karaduman, I.; Er, E.; Çelikkan, H.; Erk, N.; Acar, S. Room-temperature ammonia gas sensor based on reduced graphene oxide nanocomposites decorated by Ag, Au and Pt nanoparticles. *J. Alloys Compd.* **2017**, *722*, 569−578.

(40) Song, H.; Li, X.; Cui, P.; Guo, S.; Liu, W.; Wang, X. Morphology optimization of CVD graphene decorated with Ag nanoparticles as ammonia sensor. *Sens. Actuators, B* **2017**, *244*, 124−130.
(41) Zhao, M.; Yan, L.; Zhang, X.; Xu, L.; Song, Z.; Chen, P.; Dong, F.; Chu, W. Room temperature NH3 detection of Ti/graphene devices promoted by visible light illumination. *J. Mater. Chem. C* **2017**, *5*, 1113−1120.
(42) Kumar, R.; Varandani, D.; Mehta, B. R.; Singh, V. N.; Wen, Z.; Feng, X.; Müllen, K. Fast response and recovery of hydrogen sensing in Pd-Pt nanoparticle-graphene composite layers. *Nanotechnology* **2011**, *22*, 275719.
(43) Baachaoui, S.; Aldulaijan, S.; Raouafi, F.; Besbes, R.; Sementa, L.; Fortunelli, A.; Raouafi, N.; Dhouib, A. Pristine graphene covalent functionalization with aromatic aziridines and their application in the sensing of volatile amines−an ab initio investigation. *RSC Adv.* **2021**, *11*, 7070−7077.
(44) Yang, G. H.; Bao, D. D.; Liu, H.; Zhang, D. Q.; Wang, N.; Li, H. T. Functionalization of Graphene and Applications of the Derivatives. *J. Inorg. Organomet. Polym.* **2017**, *27*, 1129−1141.
(45) Iezhokin, I.; den Boer, D.; Offermans, P.; Ridene, M.; Elemans, J. A.; Adriaans, G. P.; Flipse, C. F. Porphyrin molecules boost the sensitivity of epitaxial graphene for NH3 detection. *J. Phys.: Condens. Matter* **2017**, *29*, 065001.
(46) Tang, X. H.; Mager, N.; Vanhorenbeke, B.; Hermans, S.; Raskin, J. P. Defect-free functionalized graphene sensor for formaldehyde detection. *Nanotechnology* **2017**, *28*, 055501.
(47) Greenwood, J.; Phan, T. H.; Fujita, Y.; Li, Z.; Ivasenko, O.; Vanderlinden, W.; Van Gorp, H.; Frederickx, W.; Lu, G.; Tahara, K.; et al. Covalent modification of graphene and graphite using diazonium chemistry: tunable grafting and nanomanipulation. *ACS Nano* **2015**, *9*, 5520−5535.
(48) Park, J.; Yan, M. D. Covalent Functionalization of Graphene with Reactive Intermediates. *Acc. Chem. Res.* **2013**, *46*, 181−189.
(49) Dammak, A.; Raouafi, F.; Cavanna, A.; Rudolf, P.; di Caprio, D.; Sallet, V.; Madouri, A.; Jancu, J. M. Quantum tailoring of electronic properties in covalently functionalized graphene: application to ammonia gas detection. *RSC Adv.* **2022**, *12*, 36002−36011.
(50) Kumar, R.; Ghosh, R. Selective determination of ammonia, ethanol and acetone by reduced graphene oxide based gas sensors at room temperature. *Sens. Bio-Sens. Res.* **2020**, *28*, 100336.
(51) Guo, Z.; Wang, B.; Wang, X.; Li, Y.; Gai, S.; Wu, Y.; Cheng, X. A high-sensitive room temperature gas sensor based on cobalt phthalocyanines and reduced graphene oxide nanohybrids for the ppb-levels of ammonia detection. *RSC Adv.* **2019**, *9*, 37518−37525.
(52) Zhou, X.; Wang, X.; Wang, B.; Chen, Z.; He, C.; Wu, Y. Preparation, characterization and NH3-sensing properties of reduced graphene oxide/copper phthalocyanine hybrid material. *Sens. Actuators, B* **2014**, *193*, 340−348.
(53) Bonegardt, D.; Klyamer, D.; Sukhikh, A.; Krasnov, P.; Popovetskiy, P.; Basova, T. Fluorination vs. Chlorination: Effect on the Sensor Response of Tetrasubstituted Zinc Phthalocyanine Films to Ammonia. *Chemosensors* **2021**, *9*, 137.
(54) Perdew, J. P.; Ernzerhof, M.; Burke, K. Rationale for mixing exact exchange with density functional approximations. *J. Chem. Phys.* **1996**, *105*, 9982−9985.
(55) Perdew, J. P.; Ruzsinszky, A.; Tao, J.; Staroverov, V. N.; Scuseria, G. E.; Csonka, G. I. Prescription for the design and selection of density functional approximations: more constraint satisfaction with fewer fits. *J. Chem. Phys.* **2005**, *123*, 062201.
(56) Grimme, S. Density functional theory with London dispersion corrections. *Wires Comput. Mol. Sci.* **2011**, *1*, 211−228.
(57) Grimme, S.; Antony, J.; Ehrlich, S.; Krieg, H. A consistent and accurate ab initio parametrization of density functional dispersion correction (DFT-D) for the 94 elements H-Pu. *J. Chem. Phys.* **2010**, *132*, 154104.
(58) Grimme, S.; Ehrlich, S.; Goerigk, L. Effect of the damping function in dispersion corrected density functional theory. *J. Comput. Chem.* **2011**, *32*, 1456−1465.
(59) Giannozzi, P.; Andreussi, O.; Brumme, T.; Bunau, O.; Buongiorno Nardelli, M.; Calandra, M.; Car, R.; Cavazzoni, C.; Ceresoli, D.; Cococcioni, M.; et al. Advanced capabilities for materials modelling with QUANTUM ESPRESSO. *J. Phys. Cond. Matter.* **2017**, *29*, 465901.
(60) Blochl, P. E. Projector augmented-wave method. *Phys. Rev. B: Condens. Matter* **1994**, *50*, 17953−17979.
(61) Blochl, P. E.; Forst, C. J.; Schimpl, J. Projector augmented wave method: ab initio molecular dynamics with full wave functions. *Bull. Mater. Sci.* **2003**, *26*, 33−41.
(62) Brandbyge, M.; Mozos, J.-L.; Ordejón, P.; Taylor, J.; Stokbro, K. Density-functional method for nonequilibrium electron transport. *Phys. Rev. B* **2002**, *65*, 165401.
(63) García, A.; Papior, N.; Akhtar, A.; Artacho, E.; Blum, V.; Bosoni, E.; Brandimarte, P.; Brandbyge, M.; Cerdá, J. I.; Corsetti, F.; et al. Siesta: Recent developments and applications. *J. Chem. Phys.* **2020**, *152*, 204108.
(64) Soler, J. M.; Artacho, E.; Gale, J. D.; García, A.; Junquera, J.; Ordejón, P.; Sánchez-Portal, D. The SIESTA method for *ab initio* order-*N* materials simulation. *J. Phys.: Condens. Matter* **2002**, *14*, 2745−2779.
(65) Hamann, D. R. Optimized norm-conserving Vanderbilt pseudopotentials. *Phys. Rev. B* **2013**, *88*, 085117.
(66) Schlipf, M.; Gygi, F. Optimization algorithm for the generation of ONCV pseudopotentials. *Comput. Phys. Commun.* **2015**, *196*, 36−44.
(67) Kim, J.; Lee, N.; Min, Y. H.; Noh, S.; Kim, N.-K.; Jung, S.; Joo, M.; Yamada, Y. Distinguishing Zigzag and Armchair Edges on Graphene Nanoribbons by X-ray Photoelectron and Raman Spectroscopies. *ACS Omega* **2018**, *3*, 17789−17796.
(68) Kuhne, T. D.; Iannuzzi, M.; Del Ben, M.; Rybkin, V. V.; Seewald, P.; Stein, F.; Laino, T.; Khaliullin, R. Z.; Schutt, O.; Schiffmann, F.; et al. CP2K: An electronic structure and molecular dynamics software package - Quickstep: Efficient and accurate electronic structure calculations. *J. Chem. Phys.* **2020**, *152*, 194103.
(69) VandeVondele, J.; Hutter, J. Gaussian basis sets for accurate calculations on molecular systems in gas and condensed phases. *J. Chem. Phys.* **2007**, *127*, 114105.
(70) Goedecker, S.; Teter, M.; Hutter, J. Separable dual-space Gaussian pseudopotentials. *Phys. Rev. B: Condens. Matter* **1996**, *54*, 1703−1710.
(71) Löwdin, P.-O. On the nonorthogonality problem. *Adv. Quantum Chem.* **1970**, *5*, 185−199.
(72) Li, J.-H.; Wu, J.; Yu, Y.-X. DFT exploration of sensor performances of two-dimensional WO3 to ten small gases in terms of work function and band gap changes and I-V responses. *Appl. Surface Sci.* **2021**, *546*, 149104.
(73) Rowley, D.; Steiner, H. Kinetics of diene reactions at high temperatures. *Discuss. Faraday Soc.* **1951**, *10*, 198−213.
(74) Simmie, J. M. Kinetic study of a retro Diels−Alder reaction in a single-pulse shock tube: Decyclization of 1-methylcyclohex-1-ene. *Int. J. Chem. Kinet.* **1978**, *10*, 227−231.
(75) Zhang, W.; Lu, W.-C.; Zhang, H.-X.; Ho, K. M.; Wang, C. Z. Lattice distortion and electron charge redistribution induced by defects in graphene. *Carbon* **2016**, *110*, 330−335.
(76) Harold, S. E.; Bready, C. J.; Juechter, L. A.; Kurfman, L. A.; Vanovac, S.; Fowler, V. R.; Mazaleski, G. E.; Odbadrakh, T. T.; Shields, G. C. Hydrogen-Bond Topology Is More Important Than Acid/Base Strength in Atmospheric Prenucleation Clusters. *J. Phys. Chem. A* **2022**, *126*, 1718−1728.
(77) Saeidfirozeh, H.; Shafiekhani, A.; Askari, M. B. Electron-transport and gas sensing in armchair graphene nanoribbons by density functional method. *Mater. Sci. Semicond. Process.* **2021**, *132*, 105881.
(78) Piras, A.; Ehlert, C.; Gryn'ova, G. Sensing and sensitivity: Computational chemistry of graphene-based sensors. *Wiley Interdiscip. Rev.: Comput. Mol. Sci.* **2021**, *11*, No. e1526.
(79) Milowska, K. Z.; Majewski, J. A. Graphene-Based Sensors: Theoretical Study. *J. Phys. Chem. C* **2014**, *118*, 17395−17401.

(80) Rodríguez, S. J.; Makinistian, L.; Albanesi, E. Computational study of transport properties of graphene upon adsorption of an amino acid: importance of including −NH2 and −COOH groups. *J. Comput. Electron.* **2017**, *16*, 127−132.
(81) Cusati, T.; Fiori, G.; Gahoi, A.; Passi, V.; Lemme, M. C.; Fortunelli, A.; Iannaccone, G. Electrical properties of graphene-metal contacts. *Sci. Rep.* **2017**, *7*, 5109.
(82) Nah, J.; Perkins, F. K.; Lock, E. H.; Nath, A.; Boyd, A.; Myers-Ward, R. L.; Gaskill, D. K.; Osofsky, M.; Rao, M. V. Electrical and Low Frequency Noise Characterization of Graphene Chemical Sensor Devices Having Different Geometries. *Sensors* **2022**, *22*, 1183.

https://doi.org/10.1021/acs.jpcc.3c01945
J. Phys. Chem. C 2023, 127, 15474−15485